


Estimating $\gamma\gamma$ absorption for ultrahigh-energy photons with lepton and hadron production

Giorgio Galanti^{1,*}, Fulvio Piccinini^{2,†}, Marco Roncadelli^{2,1,‡} and Fabrizio Tavecchio^{1,§}

¹INAF, Osservatorio Astronomico di Brera, Via E. Bianchi 46, I-23807 Merate, Italy

²INFN, Sezione di Pavia, Via A. Bassi 6, I-27100 Pavia, Italy

 (Received 19 December 2019; revised 19 June 2020; accepted 2 November 2020; published 1 December 2020)

The contribution to the cosmic opacity of ultra-high-energy (UHE) ($E > 10^{18}$ eV) γ rays has been computed so far for the $\gamma\gamma \rightarrow e^+e^-$ and $\gamma\gamma \rightarrow e^+e^-e^+e^-$ processes alone. We go a step further by systematically evaluating the additional opacity brought about by other leptons and hadrons. We find that the new dominant channels are those leading to the production of μ^\pm and hadrons (mainly π^\pm , π^0 , K^\pm , K^0 , η). Our result can be expressed in terms of the probability distribution for the interaction lengths. For a few interaction lengths such a probability gets reduced by up to 20%–30% with respect to current estimates.

DOI: [10.1103/PhysRevD.102.123004](https://doi.org/10.1103/PhysRevD.102.123004)

I. INTRODUCTION

The propagation of γ -rays in the Universe is severely limited by absorption through the interaction with soft radiation backgrounds, leading to the production of particle/antiparticle pairs [1]. The most commonly considered reaction is the e^\pm pair production $\gamma\gamma \rightarrow e^+e^-$, which starts to become important above few tens of GeV for sources at cosmological distances. Below energies $\simeq 10^{14}$ eV the main targets are the IR-optical-UV photons belonging to the so-called extragalactic background light (EBL), the fossil record of light produced by stars along the whole cosmic history (for a review, see [2]). At energies above $\simeq 10^{14}$ eV the major source of opacity is instead the cosmic microwave background (CMB), which restricts the mean free path of γ rays of energy $\simeq 10^{15}$ eV to about 10 kpc (see e.g., [3]). Ultra-high-energy (UHE) γ rays with energies above 10^{18} eV interact with the Rayleigh-Jeans tail of the CMB spectrum and the cosmic radio background (RB). The potential detection of UHE photons is quite relevant, since they provide a natural probe for several fundamental processes [4,5]. Actually, UHE photons are the by-product of the photo-meson reactions which restrict the propagation of UHE cosmic rays to $\simeq 100$ Mpc (the so-called GZK radius) [6,7]. Currently, only upper bounds on the UHE flux have been derived [4]. Because photons produced at cosmic distances suffer from absorption during their propagation to the Earth, any comparison of these upper limits with theoretical expectations must rely upon the accurate estimate of the cosmic opacity at UHE [7,8].

So far, the photon interaction length λ_γ at UHE has been modeled by using specific codes [8] which, however, include only pure QED effects, and often consider only the $\gamma\gamma \rightarrow e^+e^-$ process. The aim of this paper is to quantify the relevance for the UHE photon opacity—namely the absorption probability—brought about by hadron-producing and lepton-producing reactions. They are kinematically allowed for UHE photons because of the large energies available in the center-of-mass (CM) frame \mathcal{S}_{CM} . These processes have been considered rather cursorily many years ago within the framework of effective treatments (see e.g., [9] and references therein). Specifically, our goal is to compute them in a systematic fashion and in the light of the state-of-the-art knowledge. Accordingly, we shall denote by $\lambda_{\gamma,\text{tot}}$ the total photon interaction length. We would like to stress that the present paper is *restricted to this topic, and does not address either the origin of the UHE photons or the fate of the newly produced particles, namely secondary photons or hadrons and leptons*. Our goal can be rephrased by exploiting an analogy with quantum mechanics. Accordingly, we compute the analog of the propagator of the Schrödinger equation and not of a generic wave function, which can be derived from the knowledge of the propagator once the initial wave function is given.

The paper is organized as follows. In Sec. II we study the pair production cross section for both lepton and hadron production. In Secs. III and IV we cursorily review the calculation of the double pair production cross section, and the single neutral meson and *para*-positronium production cross sections, respectively. In Sec. V we show how to compute the interaction length and optical depth associated with a generic process. In Sec. VI we present some preliminary concepts needed to express our results, which are reported and discussed in Sec. VII. Finally, in Sec. VIII we offer our conclusions.

*gam.galanti@gmail.com

†fulvio.piccinini@pv.infn.it

‡marco.roncadelli@pv.infn.it

§fabrizio.tavecchio@inaf.it

II. PAIR PRODUCTION CROSS SECTION

Starting from lepton production, in order to get a feeling of what happens in different energy regimes, we recalculate the cross section $\sigma_{\gamma\gamma\rightarrow\bar{l}l}$ of the process $\gamma\gamma\rightarrow\bar{l}l$, where l is a generic charged lepton of mass m . The process $\gamma\gamma\rightarrow\bar{l}l$ receives contributions from t - and u -channel diagrams. We compute $\sigma_{\gamma\gamma\rightarrow\bar{l}l}$ in \mathcal{S}_{CM} where the two incident photons have four-momenta $k_1 \equiv (\omega, \mathbf{\omega})$ and $k_2 \equiv (\omega, -\mathbf{\omega})$ and the outgoing leptons have four-momenta $p_1 \equiv (\omega, \mathbf{p})$ and $p_2 \equiv (\omega, -\mathbf{p})$, with ω denoting the photon energy and \mathbf{p} the lepton three-momentum (see Fig. 1). Integrating over the total solid angle we get the total cross section [10]

$$\sigma_{\gamma\gamma\rightarrow\bar{l}l}(\omega, p) = \frac{\pi\alpha^2}{\omega^2} \left\{ \left(1 + \frac{m^2}{\omega^2} - \frac{1}{2} \frac{m^4}{\omega^4} \right) \times \ln \left[\frac{(\omega + p)^2}{m^2} \right] - \frac{p}{\omega} \left(1 + \frac{m^2}{\omega^2} \right) \right\}, \quad (1)$$

where α is the fine-structure constant.

The lepton dispersion relation $\omega^2 = p^2 + m^2$ allows us to express $\sigma_{\gamma\gamma\rightarrow\bar{l}l}$ entering Eq. (1) in terms of ω only, and by employing the Lorentz-invariant Mandelstam variable $s = (k_1 + k_2)^2 = 4\omega^2$ we can rewrite $\sigma_{\gamma\gamma\rightarrow\bar{l}l}$ in terms of s alone (see Fig. 2).

As far as the production of hadrons is concerned, the picture is much more involved because of the presence of nonperturbative effects. First detailed studies of the process $\gamma\gamma\rightarrow\text{hadrons}$ in the context of e^+e^- collider physics have been presented in [10,12], while first investigations on the $\gamma\gamma$ total hadronic cross section and its relevance for the absorption of extragalactic γ rays has been briefly discussed in [13]. In the low-energy region the hadronic cross section is dominated by pion pair production. In addition to tree-level results based on scalar QED for charged pions, refined predictions in chiral perturbation theory have been computed at one- and two-loop level in [14] and [15,16], respectively. These predictions are reliable in the region $\sqrt{s} \lesssim 500$ MeV with the higher order corrections increasing the cross section by about 20%. Also the process $\gamma\gamma\rightarrow\pi^0\pi^0$ at one- and two-loop level has been studied in [14,17]

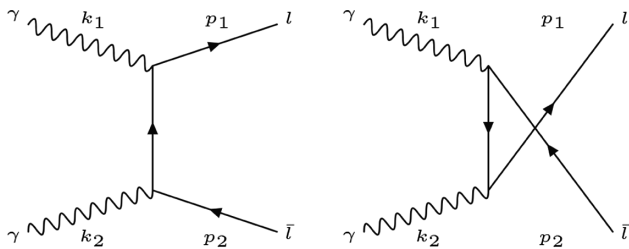


FIG. 1. Feynman diagrams in the t and u channels for the process $\gamma\gamma\rightarrow\bar{l}l$.

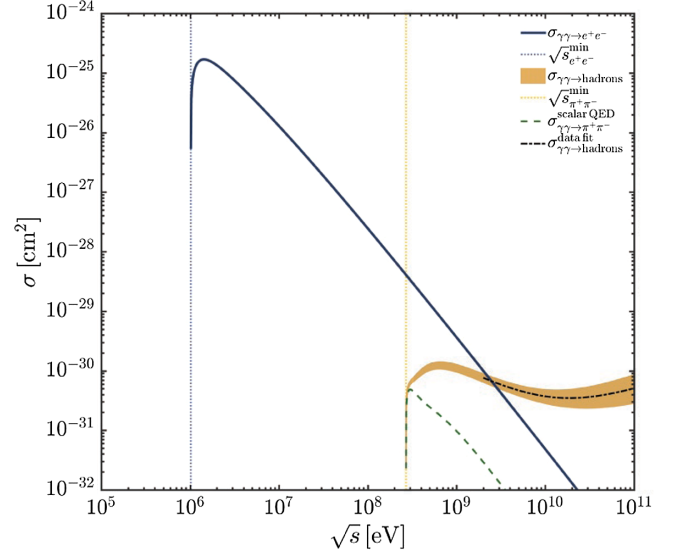


FIG. 2. Behavior of $\sigma_{\gamma\gamma\rightarrow e^+e^-}$ and $\sigma_{\gamma\gamma\rightarrow\text{hadrons}}$ cross sections and corresponding thresholds. The colored area represents the uncertainty affecting $\sigma_{\gamma\gamma\rightarrow\text{hadrons}}$. Also plotted are $\sigma_{\gamma\gamma\rightarrow\pi^+\pi^-}^{\text{scalar QED}}$ and the data fit cross section $\sigma_{\gamma\gamma\rightarrow\text{hadrons}}^{\text{data fit}}$ [11].

and [18,19], respectively, with the total contribution not exceeding the cross section for charged pion production by about 10%. The peak of the total cross section (charged plus neutral pion pairs) shows up at $\sqrt{s} \simeq 300$ MeV, with a value of about 600 nb.

The energy region $500 \text{ MeV} \lesssim \sqrt{s} \lesssim 1.5 \text{ GeV}$ is populated by hadronic resonances with $J^{PC} = 0^{++}$ [20], which couple to the initial photon pair and complicate the picture. The cross section has been measured at flavor factories for different exclusive channels, with event selection cuts on the polar angle of the hadronic decay products (see e.g., [21–23]).

The total hadronic $\gamma\gamma$ cross section in the energy region $\sqrt{s} \gtrsim 1.5 \text{ GeV}$ can be described by various models with their inherent uncertainties (for a review see [11] and references therein). But for CM energies up to 200 GeV—thus spanning two orders of magnitude in energy—the $\gamma\gamma$ hadronic cross section has been measured at large electron-positron collider [24,25] and a Regge-inspired parametrization of the type

$$\sigma_{\gamma\gamma\rightarrow\text{hadrons}}^{\text{data fit}}(s) = A s^\epsilon + B s^{-\eta} \quad (2)$$

has been fitted to the data.

Our predictions for the total hadronic $\gamma\gamma$ cross section in the region $\sqrt{s} \geq 1.5 \text{ GeV}$ are obtained from the latter parametrization, with the following parameter values: $A = 51 \pm 14 \text{ nb}$, $B = 1132 \pm 158 \text{ nb}$, $\epsilon = 0.240 \pm 0.032$ and $\eta = 0.358$. In the low-energy regime we stick to the tree-level scalar QED prediction [10]

$$\sigma_{\gamma\gamma\rightarrow\pi^+\pi^-}^{\text{scalar QED}}(\omega, p) = \frac{\pi\alpha^2}{4\omega^2} \left\{ 2 \left(1 + \frac{m_{\pi^\pm}^2}{\omega^2} \right) \frac{p}{\omega} - \frac{m_{\pi^\pm}^2}{\omega^2} \left(2 - \frac{m_{\pi^\pm}^2}{\omega^2} \right) \ln \left[\frac{(\omega + p)^2}{m_{\pi^\pm}^2} \right] \right\}, \quad (3)$$

where m_{π^\pm} is the π^\pm mass. We multiply the cross section by a K factor in order to reproduce the prediction of two-loop chiral perturbation theory of about 600 nb at $\sqrt{s} \simeq 300$ MeV. We then smoothly connect these predictions in the intermediate region, including the shape due to the hadronic resonances within our uncertainty band. The resulting cross section as a function of the CM energy is plotted in Fig. 2, with the threshold given by $2m_\pi$.

In order to evaluate the interaction length λ_γ of UHE photons interacting with soft background photons, we work in a generic inertial reference frame \mathcal{S} , wherein E denotes the energy of the hard photon and ϵ that of the soft background photon. As a result, s reads

$$s = 4\omega^2 = 2E\epsilon(1 - \cos\varphi), \quad (4)$$

where φ is the angle between the two photon three-momenta. In order to translate $\sigma_{\gamma\gamma\rightarrow\bar{l}l}$ and $\sigma_{\gamma\gamma\rightarrow\text{hadrons}}$ from \mathcal{S}_{CM} to \mathcal{S} , we use the fermion dispersion relation and Eq. (4), thereby obtaining them as written in \mathcal{S} and denoted by $\sigma_{\gamma\gamma\rightarrow\bar{l}l}(E, \epsilon, \varphi)$ and $\sigma_{\gamma\gamma\rightarrow\text{hadrons}}(E, \epsilon, \varphi)$, respectively, which will be used to compute the corresponding contribution $\lambda_{\gamma,\gamma\gamma\rightarrow\bar{l}l}$ and $\lambda_{\gamma,\gamma\gamma\rightarrow\text{hadrons}}$ to $\lambda_{\gamma,\text{tot}}$.

III. DOUBLE PAIR PRODUCTION

At very high energies the e^+e^- double pair-production cross section can be well approximated by [9,26]

$$\sigma_{\gamma\gamma\rightarrow e^+e^-e^+e^-}(s) = \frac{\alpha^4}{\pi m_e^2} \left(\frac{175}{36} \zeta(3) - \frac{19}{18} \right) \left(1 - \frac{16m_e^2}{s} \right)^6, \quad (5)$$

where m_e is the electron mass and $\zeta(\cdot)$ is the Riemann zeta function. The $4m_e$ threshold has been taken into account by means of a step function. This simplified approach becomes unreliable in the region close to the threshold. However, we have checked that, by changing the energy threshold of the step function from $s_0 = 4m_e$ to $100s_0$, $\lambda_{\gamma,\gamma\gamma\rightarrow e^+e^-e^+e^-}$ is unaffected in the energy region of the UHE photons above 10^{18} eV within the \mathcal{S} frame we are working in.

The asymptotic cross section for $\gamma\gamma \rightarrow e^+e^-\mu^+\mu^-$ has been computed in [26–29], finding values of about three orders of magnitude lower than $\sigma_{\gamma\gamma\rightarrow e^+e^-e^+e^-}$, thus completely negligible for our purposes.

IV. SINGLE NEUTRAL MESON PRODUCTION

We consider here the production of the neutral mesons π^0 , η , η' and η_c induced by the $\gamma\gamma$ scattering.

For π^0 the dominant decay mode is into two photons $\pi^0 \rightarrow \gamma\gamma$. Here, we consider the inverse process of single π^0 production $\gamma\gamma \rightarrow \pi^0$ whose cross section is

$$\sigma_{\gamma\gamma\rightarrow\pi^0}(s) = \frac{8\pi^2}{m_{\pi^0}} \Gamma_{\pi^0\rightarrow\gamma\gamma} \delta(s - m_{\pi^0}^2), \quad (6)$$

where $\Gamma_{\pi^0\rightarrow\gamma\gamma} = 7.82$ eV is the experimental π^0 decay rate [20].

For η , η' and η_c the situation is similar, apart from the fact that not always the $\gamma\gamma$ channel represents the dominant decay mode. In Eq. (6) we must replace m_{π^0} and $\Gamma_{\pi^0\rightarrow\gamma\gamma}$ with the corresponding quantities for η , η' and η_c . For the masses we take $m_\eta = 548$ MeV, $m_{\eta'} = 958$ MeV and $m_{\eta_c} = 2984$ MeV while for the $\gamma\gamma$ decay rates $\Gamma_{\eta\rightarrow\gamma\gamma} = 0.51$ keV, $\Gamma_{\eta'\rightarrow\gamma\gamma} = 4.3$ keV and $\Gamma_{\eta_c\rightarrow\gamma\gamma} = 5$ keV [20].

The cross section for the production of *para*-positronium (p -Ps) via $\gamma\gamma \rightarrow p$ -Ps possesses the same functional form of Eq. (6) with m_{π^0} replaced by $m_{p\text{-Ps}} \simeq 2m_e$ and $\Gamma_{\pi^0\rightarrow\gamma\gamma}$ by $\Gamma_{p\text{-Ps}\rightarrow\gamma\gamma} = 5.29 \times 10^{-6}$ eV [30].

V. PHOTON INTERACTION LENGTH

Denoting by E_0 the observed hard photon energy in \mathcal{S} , the inverse of the interaction length $\lambda_\gamma(E_0, z)$ at redshift z for a hard photon of energy $E = (1+z)E_0$ interacting with background soft photons of energy ϵ is computed by multiplying the background spectral number density $n_\gamma(\epsilon(z), z)$ by the cross section of two interacting photons $\sigma_{\gamma\gamma}(E(z), \epsilon(z), \varphi)$, and next integrating over φ and $\epsilon(z)$ [1,31]. The result is

$$\lambda_\gamma^{-1}(E_0, z) = \int_{-1}^1 d(\cos\varphi) \frac{1 - \cos\varphi}{2} \times \int_{\epsilon_{\text{thr}}(E(z), \varphi)}^\infty d\epsilon(z) n_\gamma(\epsilon(z), z) \sigma_{\gamma\gamma}(E(z), \epsilon(z), \varphi), \quad (7)$$

while the optical depth $\tau_\gamma(E_0, z)$ reads

$$\tau_\gamma(E_0, z) = \frac{1}{H_0} \int_0^z dz' \frac{\lambda_\gamma^{-1}(E_0, z')}{(1+z')[\Omega_\Lambda + \Omega_M(1+z')^3]^{1/2}}. \quad (8)$$

In the standard Λ CDM cosmological model we take for definiteness $H_0 = 70$ km s $^{-1}$ Mpc $^{-1}$ —which in natural units reads $H_0 = 1.50 \times 10^{-33}$ eV—while $\Omega_\Lambda = 0.7$ and $\Omega_M = 0.3$. In addition, we have

$$\epsilon_{\text{thr}}(E, \varphi) \equiv \frac{m_{\text{thr}}^2}{2E(1 - \cos \varphi)}, \quad (9)$$

where m_{thr} is the total mass of the produced particles: for leptons m_{thr} is the mass of two/four leptons, for hadrons m_{thr} is the mass of the two produced mesons, the minimum being $2m_\pi$. For single meson and *para*-positronium production m_{thr} is the meson and *para*-positronium mass, respectively.

Concerning $n_\gamma(\epsilon(z), z)$ of the soft photon background we consider the EBL, the CMB and the RB. For the EBL we adopt here the model of Gilmore *et al.* [32] mainly because the values of $n_\gamma(\epsilon(z), z)$ are tabulated. Similar results can be obtained e.g., by employing the model of Franceschini and Rodighiero [33]. For the CMB we consider the standard temperature $T = 2.73$ K, and concerning the RB we use the most recent available data with two low-frequency cutoffs [34].

(1) One placed at 2 MHz, called *intermediate* RB.

(2) Another placed at 10 MHz, called *minimal* RB.

They differ by a considerable extent, and their importance for the analysis contained in this paper will be discussed in Sec. VIII.

VI. TOWARDS THE RESULTS

We are now in a position to evaluate the contribution to the interaction length $\lambda_{\gamma, \text{tot}}$ arising from all considered

processes, namely $\lambda_{\gamma, \gamma\gamma \rightarrow l\bar{l}}$ ($l = e, \mu, \tau$), $\lambda_{\gamma, \gamma\gamma \rightarrow \text{hadrons}}$, $\lambda_{\gamma, \gamma\gamma \rightarrow e^+e^-e^+e^-}$, $\lambda_{\gamma, \gamma\gamma \rightarrow \pi^0, \eta, \eta', \eta_c}$ and $\lambda_{\gamma, \gamma\gamma \rightarrow p\text{-Ps}}$.

In Fig. 3 we plot the interaction length at $z = 0$ of all processes considered so far, along with the total interaction length which is defined as

$$\lambda_{\gamma, \text{tot}} \equiv \left(\sum_i \lambda_{\gamma, i}^{-1} \right)^{-1}, \quad (10)$$

where $\{\lambda_{\gamma, i}\}$ are the interaction lengths pertaining to each process considered above. Moreover, any quantity referring to every such process will henceforth be labeled by i . The shadowed area in Fig. 3 represents the uncertainty in $\lambda_{\gamma, \text{tot}}$ arising from that affecting $\sigma_{\gamma\gamma \rightarrow \text{hadrons}}$.

In order to figure out the relative importance of each considered processes, it is compelling to compute the associated *photon survival probabilities* $\{P_{\gamma, i}\}$, which enter the quantity \mathcal{F} defined in Eq. (18) below, and ultimately in Fig. 4. They are related to the optical depths $\{\tau_{\gamma, i}\}$ by

$$P_{\gamma, i} = e^{-\tau_{\gamma, i}}, \quad (11)$$

and hence—since the various considered channels are independent—the probability calculus implies that the total survival probability is

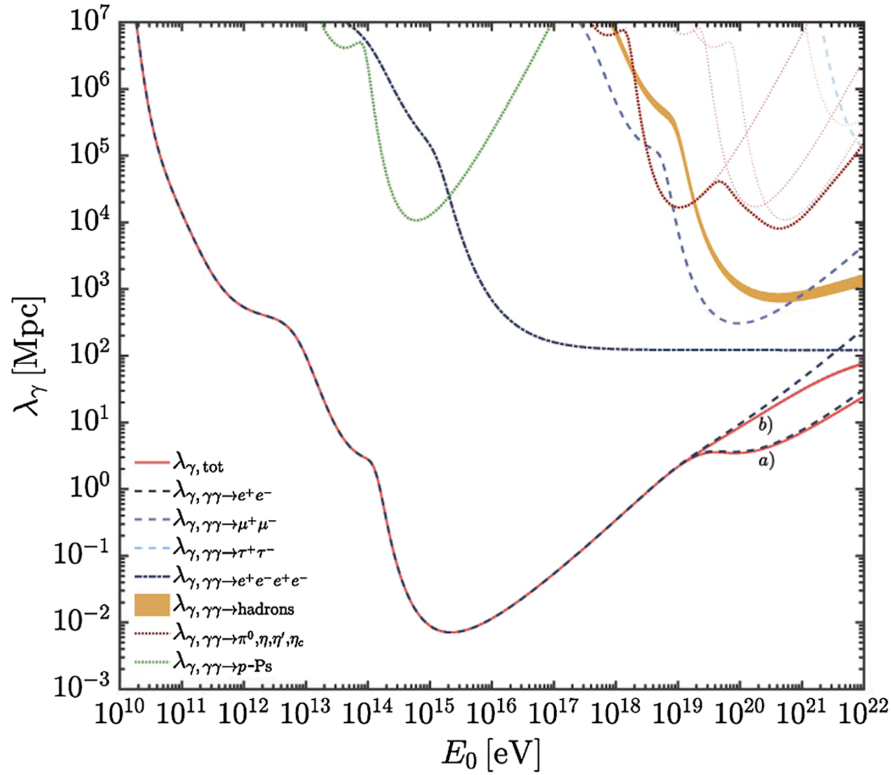


FIG. 3. Interaction length $\lambda_{\gamma, \text{tot}}$ for all considered processes calculated at redshift $z = 0$. The colored area represents the uncertainty on $\lambda_{\gamma, \text{tot}}$ corresponding to the $\gamma\gamma \rightarrow \text{hadrons}$ channel caused by the uncertainty affecting $\sigma_{\gamma\gamma \rightarrow \text{hadrons}}$. Curves a) and b) correspond to the RBs defined in Sec. V for an intermediate and a minimal RB, respectively.

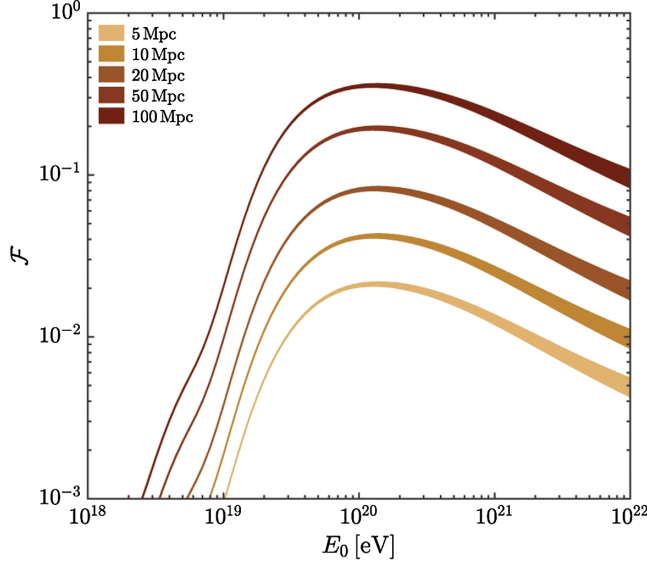


FIG. 4. At distances $5 \text{ Mpc} \leq D \leq 100 \text{ Mpc}$, we show the fractional relevance $\mathcal{F} \equiv |P_{\gamma,\text{tot}} - P_{\gamma,\text{old}}|/P_{\gamma,\text{old}}$ of the new considered channels with respect to $P_{\gamma,\text{old}}$ for any choice of the RB below $E_0 \simeq 10^{22}$ eV (since $\mathcal{F} = 1 - P_{\gamma,\text{new}}$, see the text for more details). The width of the curves reflects the uncertainty affecting $\sigma_{\gamma\gamma \rightarrow \text{hadrons}}$ shown in Fig. 3.

$$P_{\gamma,\text{tot}} = \prod_i P_{\gamma,i}, \quad (12)$$

so that the *total* optical depth $\tau_{\gamma,\text{tot}}$ is similarly related to $P_{\gamma,\text{tot}}$ as

$$P_{\gamma,\text{tot}} = e^{-\tau_{\gamma,\text{tot}}}. \quad (13)$$

Even though the calculations in Eqs. (7) and (8) are exact in cosmology, in order to express $\tau_{\gamma,i}$ in terms of $\lambda_{\gamma,i}$ we can employ—rather than Eq. (8)—the expression

$$\tau_{\gamma,i} = \frac{D}{\lambda_{\gamma,i}}, \quad (14)$$

where D denotes the total covered distance. We remark that Eq. (14) is a very good approximation, since the GZK effect [6] forces us to work in the *local* Universe—conventionally defined by the condition $z \lesssim 0.2$ —corresponding to distances $d \lesssim 850 \text{ Mpc}$. Thus, thanks to Eqs. (10), (11), (12), (13), and (14), the total optical depth turns out to be

$$\tau_{\gamma,\text{tot}} \equiv \sum_i \tau_{\gamma,i} = D \sum_i \frac{1}{\lambda_{\gamma,i}} = \frac{D}{\lambda_{\gamma,\text{tot}}}. \quad (15)$$

Nonetheless, we stress that the values of $\lambda_{\gamma,i}$ and $\tau_{\gamma,i}$ entering our calculations have been computed by means of Eqs. (7) and (8).

In view of our subsequent developments, it is quite illuminating to denote by $\tau_{\gamma,\text{old}}$ the optical depth referring to the $\gamma\gamma \rightarrow e^+e^-$ and $\gamma\gamma \rightarrow e^+e^-e^+e^-$ processes, and likewise to denote by $\tau_{\gamma,\text{new}}$ the optical depth associated with the new considered channels. The corresponding photon survival probabilities are evidently

$$P_{\gamma,\text{old}} \equiv e^{-\tau_{\gamma,\text{old}}}, \quad (16)$$

and

$$P_{\gamma,\text{new}} \equiv e^{-\tau_{\gamma,\text{new}}}. \quad (17)$$

It is also instrumental to compare the difference between our result $P_{\gamma,\text{tot}}$ and the standard one $P_{\gamma,\text{old}}$. This task can be accomplished by defining the *fractional relevance*

$$\mathcal{F} \equiv \frac{|P_{\gamma,\text{tot}} - P_{\gamma,\text{old}}|}{P_{\gamma,\text{old}}} \quad (18)$$

of the new considered channels with respect to $P_{\gamma,\text{old}}$. Note that \mathcal{F} can be recast in the form

$$\mathcal{F} = 1 - P_{\gamma,\text{new}}. \quad (19)$$

To see this, we start by replacing \mathcal{F} in Eq. (18) with

$$\mathcal{F} = 1 - \frac{P_{\gamma,\text{tot}}}{P_{\gamma,\text{old}}}, \quad (20)$$

since the new channels lower $P_{\gamma,\text{tot}}$ with respect to $P_{\gamma,\text{old}}$. Next, we obviously have

$$P_{\gamma,\text{tot}} = P_{\gamma,\text{old}} P_{\gamma,\text{new}}, \quad (21)$$

which inserted into (20) returns Eq. (19). The advantage of Eq. (19) is to show that \mathcal{F} is *independent* of the standard process $\gamma\gamma \rightarrow e^+e^-$ for which the RB becomes preminent for $E_0 \gtrsim 10^{19}$ eV, while the RB contribution to the new channels starts to become important for $E_0 \gtrsim 10^{22}$ eV [35,36]. As a consequence, \mathcal{F} turns out to be independent of the choice of the RB up to energies $E_0 \simeq 10^{22}$ eV. The quantity \mathcal{F} is plotted at several distances ($5 \text{ Mpc} \leq D \leq 100 \text{ Mpc}$) in Fig. 4.

As we can see from Fig. 3, the most important channels in addition to $\gamma\gamma \rightarrow e^+e^-$ and $\gamma\gamma \rightarrow e^+e^-e^+e^-$ are those leading to the production of hadrons and of μ^\pm , while the production of τ^\pm is less important. The single neutral meson production that takes π^0 , η , η' and η_c into account does not play any significant role as compared to the above-mentioned processes: only around $E_0 \sim 5 \times 10^{18}$ eV represents it the leading contribution among those that must be added to the processes $\gamma\gamma \rightarrow e^+e^-$ and $\gamma\gamma \rightarrow e^+e^-e^+e^-$. The *para*-positronium production is the most important

channel after $\gamma\gamma \rightarrow e^+e^-$ around 10^{14} eV $\lesssim E_0 \lesssim 10^{15}$ eV but its correction to the process $\gamma\gamma \rightarrow e^+e^-$ is totally irrelevant for UHE photons.

Let us assume that the UHE photon energy is around $E_0 = 10^{20}$ eV, where the effect of the new channels becomes maximal (see Fig. 3). Then from the above expressions of the cross sections for the various channels, we see that—in the isotropic case—the UHE photons primarily interact with soft photons of energy ϵ_0 such that: (i) $\epsilon_0 \simeq 10^{-8}$ eV (RB) for the $\gamma\gamma \rightarrow e^+e^-$ channel, (ii) $\epsilon_0 \simeq 6 \times 10^{-4}$ eV (exact peak of the CMB) for $\gamma\gamma \rightarrow e^+e^-e^+e^-$, (iii) $\epsilon_0 \simeq 4 \times 10^{-4}$ eV (close to the CMB peak) for $\gamma\gamma \rightarrow \mu^+\mu^-$ and (iv) $\epsilon_0 \simeq 7 \times 10^{-4}$ eV (close to the CMB peak) for $\gamma\gamma \rightarrow$ hadrons, as far as the leading processes are concerned.

VII. RESULTS

We are finally in a position to quantify our results. It goes without saying that the observable quantity would be the flux (in our analogy the wave function), but in the total lack of knowledge of the initial flux (in the above analogy, the initial wave function), the best we can do is to compute the photon survival probabilities for *primary* UHE photons (the analog of the propagator).

Realistically, we expect UHE photons with energy around $E_0 \simeq 10^{20}$ eV to travel a few interaction lengths $\lambda_{\gamma,\text{tot}}$. According to Eq. (15) we have $D = \tau_{\gamma,\text{tot}}\lambda_{\gamma,\text{tot}}$. Although $\tau_{\gamma,\text{tot}}$ can take any positive value, in order to get a feeling of what goes on we have to commit ourselves with a few suitable benchmark values of $\tau_{\gamma,\text{tot}}$, which—on account of the previous equation—translate into different values of the covered distance D , whose corresponding photon survival probability is given by Eq. (13). Thus, for $\tau_{\gamma,\text{tot}} = n$ —where n is a benchmark value—a distance $D = n\lambda_{\gamma,\text{tot}}$ will be travelled, with associated photon survival provability

$$P_{\gamma,\text{tot}}(D = n\lambda_{\gamma,\text{tot}}) = e^{-n}, \quad (22)$$

owing to Eq. (13).

We believe that the simplest way to show the change brought about by the inclusion of the new channels—which can be read off from Figs. 3 and 4—amounts to compare $P_{\gamma,\text{tot}}$ to $P_{\gamma,\text{old}}$ for different numbers of the interaction length, which clearly changes the value of \mathcal{F} . Because of the great uncertainty in the RB mentioned at this end of Sec. V (more about this in Sec. VIII), we shall report the values of $P_{\gamma,\text{tot}}$ for the cases a) and b), respectively: as we shall see, $P_{\gamma,\text{tot}}$ turns out to be considerably smaller in case a) than in case b).

We proceed along the following strategy. First, from Fig. 3 we read off the value of $\lambda_{\gamma,\text{tot}}$ in cases a) and b), and next we consider a particular number of interaction length $\lambda_{\gamma,\text{tot}}$, so that the resulting total distance turns out to be

$D = n\lambda_{\gamma,\text{tot}}$. Finally, we compare $D = n\lambda_{\gamma,\text{tot}}$ —for both choices a) and b) of the RB—with the different distances reported in Fig. 4 pertaining to \mathcal{F} . In this way, we quantify how much $P_{\gamma,\text{tot}}$ becomes smaller than $P_{\gamma,\text{old}}$ for several distances.

Specifically, for a distance of $n = 1$ interaction length $P_{\gamma,\text{tot}}$ gets smaller than $P_{\gamma,\text{old}} \simeq 0.37$ by a factor \mathcal{F} roughly between 2% and 5%. Similarly, for $n = 2$ interaction lengths $P_{\gamma,\text{tot}}$ is smaller than $P_{\gamma,\text{old}} \simeq 0.14$ by a factor \mathcal{F} of roughly between 4% and 8%. Further, for $n = 4.6$ interaction lengths $P_{\gamma,\text{tot}}$ becomes smaller than $P_{\gamma,\text{old}} \simeq 0.01$ by a factor \mathcal{F} roughly between 10% and 20%. Finally, for $n = 7$ $P_{\gamma,\text{tot}}$ gets smaller than $P_{\gamma,\text{old}} \simeq 0.001$ by a factor \mathcal{F} roughly between 15% and 30%.

VIII. CONCLUSIONS

So far, the contribution to the cosmic opacity of UHE ($E > 10^{18}$ eV) γ rays has been computed only for the $\gamma\gamma \rightarrow e^+e^-$ and $\gamma\gamma \rightarrow e^+e^-e^+e^-$ processes. Instead, we have evaluated the relevance of the contributions from hadron and lepton production in UHE $\gamma\gamma$ scattering, along with those arising from the single neutral mesons and the *para*-positronium production processes. As far as the hadron sector is concerned, uncertainties affecting the interaction length $\lambda_{\gamma,\gamma\gamma \rightarrow \text{hadrons}}$ give rise to an uncertainty in $\lambda_{\gamma,\text{tot}}$ which reverberates in $P_{\gamma,\text{tot}}$. But our results are sizable even in the most conservative case, namely taking the smallest value of $\sigma_{\gamma\gamma \rightarrow \text{hadrons}}$.

A point should be stressed. While the standard $\gamma\gamma \rightarrow e^+e^-$ channel is affected by the uncertainty on the level of the RB for $E_0 \gtrsim 10^{19}$ eV (the $\gamma\gamma \rightarrow e^+e^-e^+e^-$ channel is insensitive to the RB), the new considered channels are instead *independent* of RB up to $E_0 \simeq 10^{22}$ eV, as it is shown by Eq. (19) as combined with the results reported in [35,36]. Moreover, the new channels do not add any further uncertainty apart from that coming from the hadron sector, which is however subdominant. Unfortunately, the uncertainty in the level of the RB is quite high, as shown in Fig. 3 and exceeds the contribution of the new considered channels. However, future studies of the RB may hopefully decrease its uncertainty to a level where the impact of the new channels dominates over the RB uncertainty.

A further consequence of our result—whatever the RB level—is a modification of the estimated charged UHE cosmic ray flux, since the UHE photons considered in this paper arise from the photo-meson reactions.

Finally, it goes without saying that any final product of the two-photon scattering triggers an electromagnetic (EM) cascade, thereby producing secondary photons and other particles, as first realized in 1938 by Landau and Rumer [37]. We restate that the study of this topic, as well as the origin of the UHE photons, is beyond the scope of the present Paper, since here our attention is focussed *only on the UHE photon opacity*. Manifestly—when the attention

is shifted to the estimated total photon flux at lower energies—the EM cascade must be considered along with the new channels considered in the this paper.

ACKNOWLEDGMENTS

We thank Alessandro De Angelis and Massimo Gervasi for discussions and Frédéric Kapusta for useful information. We also thank the anonymous referees for help in

clarifying the presentation. G. G. and F. T. acknowledge contribution from the Grant No. INAF CTA–SKA, “Probing particle acceleration and γ -ray propagation with CTA and its precursors” and the INAF Main Stream project “High-energy extragalactic astrophysics: toward the Cherenkov Telescope Array.” The work of F. P. is supported by an INFN QFT@Colliders grant. The work of M. R. is supported by an INFN TAsP grant.

-
- [1] R. J. Gould and G. P. Schröder, *Phys. Rev.* **155**, 1408 (1967).
 [2] E. Dwek and F. Krennrich, *Astropart. Phys.* **43**, 112 (2013).
 [3] A. De Angelis, G. Galanti, and M. Roncadelli, *Mon. Not. R. Astron. Soc.* **432**, 3245 (2013).
 [4] A. Aab *et al.*, *J. Cosmol. Astropart. Phys.* 4 (2017) 009.
 [5] G. B. Gelmini, O. E. Kalashev, and D. V. Semikoz, *JETP Lett.* **106**, 1061 (2008).
 [6] K. Greisen, *Phys. Rev. Lett.* **16**, 748 (1966); G. T. Zatsepin and V. A. Kuzmin, *Sov. Phys. JETP Lett.* **4**, 78 (1966); F. W. Stecker, *Phys. Rev. Lett.* **21**, 1016 (1968).
 [7] G. Gelmini, O. Kalashev, and D. Semikoz, *J. Cosmol. Astropart. Phys.* 11 (2007) 002.
 [8] C. Heiter, D. Kuempel, D. Walz, and M. Erdmann, *Astropart. Phys.* **102**, 39 (2018).
 [9] R. Brown, W. Hunt, K. Mikaelian, and I. Muzinich, *Phys. Rev. D* **8**, 3083 (1973).
 [10] S. J. Brodsky, T. Kinoshita, and H. Terazawa, *Phys. Rev. D* **4**, 1532 (1971).
 [11] R. M. Godbole, A. De Roeck, A. Grau, and G. Pancheri, *J. High Energy Phys.* 06 (2003) 061.
 [12] V. M. Budnev, I. F. Ginzburg, G. V. Meledin, and V. G. Serbo, *Phys. Rep.* **15**, 181 (1975).
 [13] K. Terasaki-Okada, *Prog. Theor. Phys.* **49**, 349 (1973).
 [14] J. Bijnens and F. Cornet, *Nucl. Phys.* **B296**, 557 (1988).
 [15] U. Burgi, *Nucl. Phys.* **B479**, 392 (1996); *Phys. Lett. B* **377**, 147 (1996).
 [16] J. Gasser, M. A. Ivanov, and M. E. Sainio, *Nucl. Phys.* **B745**, 84 (2006).
 [17] J. F. Donoghue, B. R. Holstein, and Y. C. Lin, *Phys. Rev. D* **37**, 2423 (1988).
 [18] S. Bellucci, J. Gasser, and M. E. Sainio, *Nucl. Phys.* **B423**, 80 (1994); **B431**, 413(E) (1994).
 [19] J. Gasser, M. A. Ivanov, and M. E. Sainio, *Nucl. Phys.* **B728**, 31 (2005).
 [20] M. Tanabashi *et al.* (Particle Data Group), *Phys. Rev. D* **98**, 030001 (2018).
 [21] T. Mori *et al.* (Belle Collaboration), *Phys. Rev. D* **75**, 051101 (2007).
 [22] S. Uehara *et al.* (Belle Collaboration), *Phys. Rev. D* **78**, 052004 (2008).
 [23] S. Uehara, Gamma gamma physics at Belle, in *Proceedings at PhiPsi13, 2013, Rome, Italy*.
 [24] M. Acciarri *et al.* (L3 Collaboration), *Phys. Lett. B* **519**, 33 (2001).
 [25] G. Abbiendi *et al.* (OPAL Collaboration), *Eur. J. Phys. C* **14**, 199 (2000).
 [26] W. da Silva and F. Kapusta, *Phys. Lett. B* **718**, 577 (2012).
 [27] E. A. Kuraev, A. Schiller, and V. G. Serbo, *Nucl. Phys.* **B256**, 189 (1985).
 [28] E. A. Kuraev, A. Schiller, and V. G. Serbo, *Nucl. Phys.* **B256**, 211 (1985).
 [29] M. Masujima, *Nucl. Phys.* **B24**, 182 (1970).
 [30] S. G. Karshenboim, *Int. J. Mod. Phys. A* **19**, 3879 (2004).
 [31] G. G. Fazio and F. W. Stecker, *Nature (London)* **226**, 135 (1970).
 [32] R. Gilmore, R. Somerville, J. Primack, and A. Domínguez, *Mon. Not. R. Astron. Soc.* **422**, 3189 (2012).
 [33] A. Franceschini and G. Rodighiero, *Astron. Astrophys.* **603**, A34 (2017).
 [34] M. Gervasi, A. Tartari, M. Zannoni, G. Boella, and G. Sironi, *Astrophys. J.* **682**, 223 (2008).
 [35] Observe that the RB contribution to the *para*-positronium starts for $E_0 \simeq 5 \times 10^{17}$ eV, but this process is at least two-to-three orders of magnitude less important than the other new considered channels (see Fig. 3). Hence, it is negligible.
 [36] Note that the process $\gamma\gamma \rightarrow e^+e^-e^+e^-$ is insensitive to the RB level. Indeed, owing to the energy independence of its cross section at high energies, UHE photons interact primarily with the photons with the largest number densities, which correspond to the CMB peak.
 [37] L. D. Landau and G. Rumer, *Proc. R. Soc. A* **166**, 213 (1938).